Optimized perturbation theory in the vortex liquid of type-II superconductors

Dingping Li* and Baruch Rosenstein†
National Center for Theoretical Sciences and Electrophysics Department, National Chiao Tung University, Hsinchu 30050, Taiwan, Republic of China

(Received 19 March 2001; revised manuscript received 21 May 2001; published 19 December 2001)

We develop an optimized perturbation theory for the Ginzburg–Landau description of thermal fluctuations effects in the vortex liquids. Unlike the high temperature expansion which is asymptotic, the optimized expansion is convergent. Radius of convergence on the lowest Landau level is $a_T=-3$ in two dimensions (2D) and $a_T=-5$ in three dimensions (3D). It allows a systematic calculation of magnetization and specific heat contributions due to thermal fluctuations of vortices in strongly type-II superconductors to a very high precision. The results are in good agreement with existing Monte Carlo simulations and experiments. Limitations of various nonperturbative and phenomenological approaches are noted. In particular we show that there is no exact intersection point of the magnetization curves both in 2D and 3D.

DOI: 10.1103/PhysRevB.65.024513 PACS number(s): 74.60.−w, 74.40.+k, 74.25.Ha, 74.25.Dw

I. INTRODUCTION

Thermal fluctuations play a much larger role in high T_c superconductors than in the low temperature ones because the Ginzburg parameter Gi characterizing fluctuations is much larger.[1] In addition the presence of magnetic field and strong anisotropy in superconductors like BSCCO effectively reduces their dimensionality thereby further enhancing effects of thermal fluctuations. Under these circumstances the mean field line separating Abrikosov lattice from ''normal'' phase becomes a phase transition between vortex lattice and liquid far below the mean field phase transition line[2,1] clearly seen in both magnetization[3] and specific heat experiments.[4] Between the mean field transition line and the melting point physical quantities like the magnetization, conductivity, and specific heat depend strongly on fluctuations. Several experimental observations call for a refined precise theory. For example, a striking feature of magnetization curves intersecting at the same point (T^*,H^*) was observed in a wide rage of magnetic fields in both layered (2D or quasi-2D)[5] materials and more isotropic ones.[6] To develop a quantitative theory of these fluctuations even in the case of the lowest Landau level (LLL) corresponding to regions of the phase diagram ''close'' to H_{c2}, is a very nontrivial task and several different approaches were developed.

A long time ago Thouless and Ruggeri[7,8] proposed a perturbative expansion around a homogeneous (liquid) state in which all the ''bubble'' diagrams (see Fig. 5) are resummed. Unfortunately they proved that the series are asymptotic and although the first few terms provide accurate results at very high temperatures, the series become inapplicable for LLL dimensionless temperature $a_T \sim (T-T_{mf}(H))/(TH)^{1/2}$ smaller than 2 in 2D quite far above the melting line (believed to be located around $a_T=-12$). Generally attempts to extend the theory to lower temperatures by the Borel transform or Pade extrapolation were not successful.[9] Several nonperturbative methods have been also attempted.

Originally the RG method was proposed[2] and developed[10] although, since the transition is first order, no solutions of the RG equations can been found. The set of perturbative ''parquet'' diagrams[11] have been resummed and the large N limit have been considered.[12] Tesanovic and co-workers developed a method based on an approximate separation of the two energy scales[13] in both 2D and 3D. The larger contribution (98%) is the condensation energy, while the smaller one (2%) describes motion of the vortices. The theory explains the intersection of the magnetization curves. This question has been tackled in 2D by rather phenomenological approach in Ref. 14. Some Monte Carlo simulations are available.[15,16] Meantime experimental precision increased dramatically. New methods like measurement of magnetization using the Hall probes[3] were invented. One can achieve a precision that allows clearly to see a tiny magnetization jumps of only 0.1 Oe in BSCCO and a sharp peak in specific heat in YBCO.

In this paper we apply optimized perturbation theory (OPT) first developed in field theory[17–19] to both the 2D and 3D LLL model. It allows to obtain a convergent series (rather than asymptotic) and therefore to calculate magnetization and specific heat of vortex liquids with definite precision. The precision for various values of the LLL scaled temperature a_T are given in Tables III and IV. The radius of convergence is $a_T=-3$ in 2D and $a_T=-5$ in 3D. One the basis of this one can make several definitive qualitative conclusions. The intersection of the magnetization lines in only approximate not only in 3D (the result already observed in Monte Carlo simulation,[16]) but also in 2D. The theory by Tesanovic *et al.*[13] in 2D describes the physics remarkably well in high temperatures, but deviates on the 5–10 % precision level at $a_T=-2$. Part of these results (the 2D) has been briefly presented in Ref. 20.

The paper is organized as follows. The models are defined in Sec. II and the general OPT described in Sec. III. The 2D and the 3D calculations are described in Sec. IV. Results and comparison with other theories and experiments are given in Sec. V. We conclude in Sec. VI.

II. MODELS

A. The 2D model

To describe fluctuations of order parameter in thin films or layered superconductors one can start with the Ginzburg–Landau free energy:

$$F=L_z\int d^2x\frac{\hbar^2}{2m_{ab}}|D\psi|^2-a|\psi|^2+\frac{b'}{2}|\psi|^4, \tag{1}$$

where $\mathbf{A}=(By,0)$ describes a constant magnetic field (considered nonfluctuating) in Landau gauge and covariant derivative is defined by $\mathbf{D}\equiv\boldsymbol{\nabla}-i(2\pi/\Phi_0)\mathbf{A},\Phi_0\equiv hc/e^*$. For strongly type II superconductors like the high T_c cuprates ($\kappa\sim100$) and not too far from H_{c2} (this is the range of interest in this paper, for the detailed discussion of the range of applicability see Ref. 21) magnetic field is homogeneous to a high degree due to superposition from many vortices. For simplicity we assume $a(T)=\alpha T_c(1-t),t\equiv T/T_c$, although this temperature dependence can be easily modified to better describe the experimental $H_{c2}(T)$. The thickness of a layer is L_z.

Throughout most of the paper will use the coherence length $\xi=\sqrt{\hbar^2/(2m_{ab}\alpha T_c)}$ as a unit of length and $[dH_{c2}(T_c)/dT]T_c=\Phi_0/2\pi\xi^2$ as a unit of magnetic field. After the order parameter field is rescaled as $\psi^2\to(2\alpha T_c/b')\psi^2$, the dimensionless free energy (the Boltzmann factor) is

$$\frac{F}{T}=\frac{1}{\omega}\int d^2x\left[\frac{1}{2}|\mathbf{D}\psi|^2-\frac{1-t}{2}|\psi|^2+\frac{1}{2}|\psi|^4\right]. \tag{2}$$

The dimensionless coefficient describing the strength of fluctuations is

$$\omega=\sqrt{2\,\mathrm{Gi}}\pi^2t=\frac{m_{ab}b'}{2\hbar^2\alpha L_z}t,\mathrm{Gi}\equiv\frac{1}{2}\left(\frac{32\pi e^2\kappa^2\xi^2T_c}{c^2h^2L_z}\right)^2, \tag{3}$$

where Gi is the Ginzburg number in 2D . When $(1-t-b)/12b\ll1$, the lowest Landau level approximation can be used.[21] The model then simplifies due to the LLL constraint, $-(\mathbf{D}^2/2)\psi=(b/2)\psi$ to

$$f\equiv\frac{F}{T}=\frac{1}{\omega}\int d^2x\left[-\frac{1-t-b}{2}|\psi|^2+\frac{1}{2}|\psi|^4\right]. \tag{4}$$

This reduced model exhibits the LLL scaling. Rescaling again $x\to x/\sqrt{b},y\to y/\sqrt{b}$, and $|\psi|^2\to|\psi|^2\sqrt{b\omega/4\pi}$, one obtains

$$f=\frac{1}{4\pi}\int d^2x\left[a_T|\psi|^2+\frac{1}{2}|\psi|^4\right], \tag{5}$$

where the 2D LLL reduced temperature

$$a_T\equiv-\sqrt{\frac{4\pi}{b\omega}}\frac{1-t-b}{2} \tag{6}$$

is the only parameter in the theory.[22,7] In total, we have done the rescaling

$$|\psi|^2\to|\psi|^2\left(\frac{2\alpha T_c}{b'}\right)\left(\sqrt{\frac{b\omega}{4\pi}}\right),\quad x\to\xi x/\sqrt{b},y\to\xi y/\sqrt{b}. \tag{7}$$

We will be interested in thermodynamic properties of the model determined by partition function $Z=\int D\psi D\bar{\psi}\exp(-f)$ and will mainly study only the rescaled partition function $Z_r(a_T)=\int D\psi_r D\bar{\psi}_r\exp(-f)=Z/J$, where J is a Jacobian. Consequently to obtain, for example, the free energy density from the corresponding quantity in the rescaled model $f_{\mathrm{eff}}=-4\pi\log Z_r/V'$, one should use the following relation:

$$\begin{aligned}-\frac{T\log Z}{V}&=\frac{T}{4\pi}\frac{V'}{V}\frac{(-4\pi\log Z_rJ)}{V'}\\&=\frac{T}{2\pi}\left(\frac{\sqrt{b}}{\xi}\right)^2\log\left(\frac{8\pi\alpha T_c}{b'T}\sqrt{\frac{b\omega}{4\pi}}\right)\\&\quad+\frac{T}{4\pi}\left(\frac{\sqrt{b}}{\xi}\right)^2f_{\mathrm{eff}}.\end{aligned} \tag{8}$$

From now on we work with rescaled quantities only and relate them to measured quantities in Sec. V.

B. The 3D model

For 3D materials with asymmetry along the z axis the GL model takes a form

$$\begin{aligned}F=\int d^3x&\frac{\hbar^2}{2m_{ab}}\left|\left(\boldsymbol{\nabla}-\frac{ie^*}{\hbar c}\mathbf{A}\right)\psi\right|^2\\&+\frac{\hbar^2}{2m_c}|\partial_z\psi|^2+a|\psi|^2+\frac{b'}{2}|\psi|^4\end{aligned} \tag{9}$$

which can be again rescaled into

$$f=\frac{F}{T}=\frac{1}{\omega}\int d^3x\left[\frac{1}{2}|\mathbf{D}\psi|^2+\frac{1}{2}|\partial_z\psi|^2-\frac{1-t}{2}|\psi|^2+\frac{1}{2}|\psi|^4\right], \tag{10}$$

by $x\to\xi x,y\to\xi y,z\to\xi z/\gamma^{1/2},\psi^2\to(2\alpha T_c/b')\psi^2$, where $\gamma\equiv m_c/m_{ab}$ is anisotropy. The Ginzburg number is now given by

$$Gi\equiv\frac{1}{2}\left(\frac{32\pi e^2\kappa^2\xi T_c\gamma^{1/2}}{c^2h^2}\right)^2. \tag{11}$$

Within the LLL approximation,

$$f=\frac{F}{T}=\frac{1}{\omega}\int d^3x\left[\frac{1}{2}|\partial_z\psi|^2-\frac{1-t-b}{2}|\psi|^2+\frac{1}{2}|\psi|^4\right]. \tag{12}$$

It also possesses an LLL scaling different from the 2D one. After a rescaling $x\to x/\sqrt{b},y\to y/\sqrt{b},z\to z[(b\omega/4\pi\sqrt{2})]^{-1/3},\psi^2\to[(b\omega/4\pi\sqrt{2})]^{2/3}\psi^2$, the dimensionless free energy becomes

$$f=\frac{1}{4\pi\sqrt{2}}\int d^3x\left[\frac{1}{2}|\partial_z\psi|^2+a_T|\psi|^2+\frac{1}{2}|\psi|^4\right]. \tag{13}$$

The 3D reduced temperature is

$$a_T=-\left(\frac{b\omega}{4\pi\sqrt{2}}\right)^{-2/3}\frac{1-t-b}{2}. \tag{14}$$

The relation between the original and scaled quantity (the 3D Jacobian contains an ultraviolet divergent term which cancels the corresponding one loop divergence and is not written here) is

$$-\frac{T\log Z}{V}=\frac{T}{4\pi\sqrt{2}}\frac{V'}{V}\frac{(-4\pi\sqrt{2}\log Z_r J)}{V'}$$
$$=\frac{T}{4\pi}\frac{\sqrt{\gamma}b}{\xi^3}\left(\frac{b\omega}{4\pi\sqrt{2}}\right)^{1/3}f_{\rm eff}. \tag{15}$$

III. GENERAL IDEA OF THE OPTIMIZED GAUSSIAN PERTURBATION THEORY FOR SCALAR FIELDS

We will use a variant of OPT, the optimized Gaussian series[19] to study the vortex liquid. It is based on the ''principle of minimal sensitivity'' idea,[17] first introduced in quantum mechanics. Any perturbation theory starts from dividing the Hamiltonian into a solvable ''large'' part and a perturbation. Since we can solve any quadratic Hamiltonian we have a freedom to choose ''the best'' such quadratic part. Quite generally such an optimization converts an asymptotic series into a convergent one (see a comprehensive discussion, references and a proof in Ref. 19). Here we describe the implementation of the OPT idea using a simple model of a real scalar field ϕ,

$$f=\tfrac{1}{2}\phi D^{-1}\phi+V(\phi), \tag{16}$$

where $D^{-1}=-\nabla^2+m^2$ is considered as a matrix in the function space. The free energy is divided into the ''large'' quadratic part and a perturbation introducing variational parameter function G^{-1}:

$$f=K+\alpha v,$$
$$K=\tfrac{1}{2}\phi G^{-1}\phi, v=f-\tfrac{1}{2}\phi G^{-1}\phi. \tag{17}$$

Here the auxiliary parameter α was introduced to generate a perturbation theory. It will be set to one at the end of the calculation. Expanding the logarithm of the statistical sum to order α^{n+1},

$$Z=\int \mathcal{D}\phi\exp(-K)\exp(-\alpha v)$$
$$=\int \mathcal{D}\phi\sum_{i=0}\frac{1}{i!}(\alpha v)^i\exp(-K),$$
$$\tilde{f}_n[G]=-\log Z$$
$$=-\log\left[\int \mathcal{D}\phi\exp(-K)\right]-\sum_{i=1}^{n+1}\frac{(-\alpha)^i}{i!}\langle v^i\rangle_K, \tag{18}$$

where $\langle\,\rangle_K$ denotes the sum of all the connected Feynman diagrams with G as a propagator and then taking $\alpha\to 1$, we obtain a functional of G. To define the nth order OPT approximant f_n one minimizes $\tilde{f}_n[G]$ with respect to G:

$$f_n=\min_G \tilde{f}_n[G]. \tag{19}$$

The leading order of this expansion, the Gaussian approximation, has been used since early days of quantum mechanics and in particular was popularized by Feynman.[23] The higher orders however were defined and explored only more recently. Until now the method has been applied and comprehensively investigated in quantum mechanics only (Ref. 19 and references therein) although attempts in field theory have been made.[17]

IV. OPT IN THE GINZBURG–LANDAU MODEL

A. 2D

Due to the translational symmetry of the vortex liquid there is only one variational parameter, ε, in the free energy defined by

$$K=\frac{\varepsilon}{4\pi}|\psi|^2,$$
$$v=+\frac{\alpha}{4\pi}\left[a_H|\psi|^2+\frac{1}{2}|\psi|^4\right] \tag{20}$$

where $a_H\equiv a_T-\varepsilon$. It is convenient to use the quasimomentum eigenfunctions similar to those used extensively in the vortex lattice:

$$\varphi_{\mathbf{k}}=\sqrt{\frac{2\pi}{\sqrt{\pi}a_\triangle}}\sum_{l=-\infty}^{\infty}\exp\left\{i\left[\frac{\pi l(l-1)}{2}+\frac{2\pi(x-k_y)}{a_\triangle}l-xk_x\right]\right.$$
$$\left.-\frac{1}{2}\left(y+k_x-\frac{2\pi}{a_{\triangle up}}l\right)^2\right\}, \tag{21}$$

where $a_\triangle=\sqrt{4\pi/\sqrt{3}}$. We expand

$$\psi(x)=\int_{\mathbf{k}(\sqrt{2\pi})^2}\varphi_{\mathbf{k}}(x)\psi(k). \tag{22}$$

Then the propagator in the quasimomentum basis is

$$\langle\psi(k)\psi(l)\rangle=\frac{4\pi}{\varepsilon}\delta(k+l). \tag{23}$$

In the coordinate space

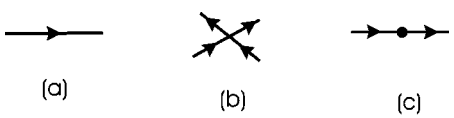

FIG. 1. Feynman rules for OPE: (a), (b), (c) are propagator, the four-line vertex and the mass insertion, respectively.

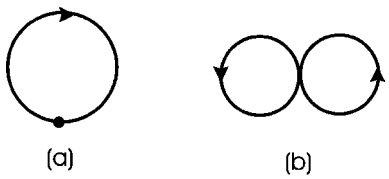

FIG. 2. Feynman diagrams for Gaussian $(n=)0$ free energy $\tilde{f}_0[G]$ prior to minimization.

$$\langle \psi^*(x_1,y_1)\psi(x_2,y_2)\rangle = \frac{2}{\varepsilon}\exp\left[-\frac{i}{2}(x_1-x_2)(y_1+y_2)\right] \times\exp\left\{-\frac{1}{4}[(x_1-x_2)^2+(y_1-y_2)^2]\right\}. \quad (24)$$

The Feynman rules are given in Fig. 1. We have a propagator denoted by a directed line, Fig. 1(a), connecting two points (x_1,y_1) to (x_2,y_2). For the first term in v, we have a vertex represented by a dot on a line, Fig. 1(c) with a value of $(\alpha/4\pi)a_H$. The second term is a four line vertex, Fig. 1(b), with a value of $(\alpha/4\pi)^{\frac{1}{2}}$. To calculate the effective energy density $f_{\rm eff}=-4\pi\ln Z$, we draw all the connected vacuum diagrams. Then one of the coordinates is fixed, and all the others are integrated out. We calculated directly diagrams up to the three loop order shown on Figs. 2, 3, and 4 with the following result:

$$\tilde{f}_0=2*\left(\frac{2}{\varepsilon^2}+\frac{a_H}{\varepsilon}+\log\frac{\varepsilon}{4\pi^2}\right),$$

$$\tilde{f}_1=\tilde{f}_0-\frac{1}{\varepsilon^4}(18+8a_H\varepsilon+a_H^2\varepsilon^2),$$

$$\tilde{f}_2=\tilde{f}_1+\frac{2}{9\varepsilon^6}(662+324a_H\varepsilon+54a_H^2\varepsilon^2+3a_H^3\varepsilon^3). \quad (25)$$

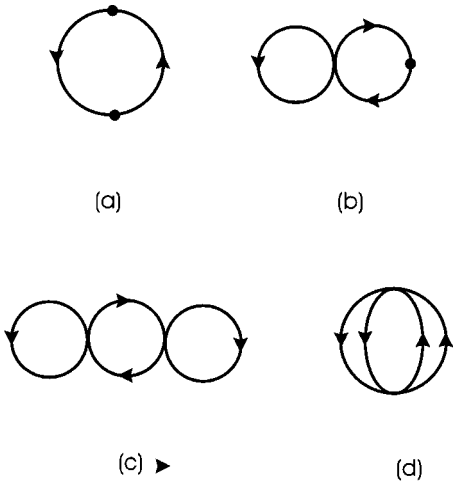

FIG. 3. Additional (to those in Fig. 2) Feynman diagrams for post-Gaussian $(n=1)$ free energy $\tilde{f}_1[G]$ prior to minimization.

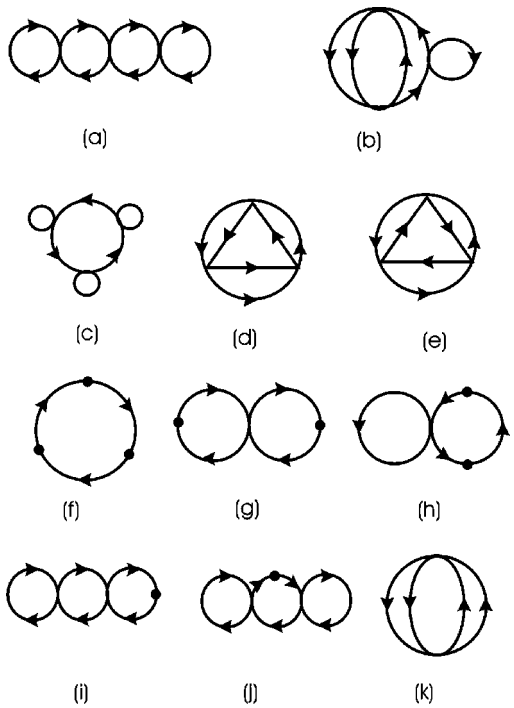

FIG. 4. Additional (to those in Figs. 2 and 3) Feynman diagrams for $n=2$ free energy $\tilde{f}_2[G]$ prior to minimization.

However to take advantage of the existing long series of the nonoptimized Gaussian expansion, we found a relation of the OPE to these series. Originally Thouless and Ruggeri calculated these series $f_{\rm eff}$ to sixth order, but it was subsequently extended to 12th by Hikami *et al.*[24] and to 13th by Hu and MacDonald.[25] It can be presented using variable x introduced by Thouless and Ruggeri,[7]

$$x=\frac{1}{\varepsilon^2},\quad \varepsilon=\frac{1}{2}(a_T+\sqrt{a_T^2+16}), \quad (26)$$

as follows:

$$f_{\rm eff}=2\log\frac{\varepsilon}{4\pi^2}+2f_{\rm 2D}(x), \quad (27)$$

$$f_{\rm 2D}(x)=\sum_{n=1}^{\infty} c_n x^n. \quad (28)$$

The coefficients are given in Table. I. We can obtain all the OPT diagrams which do not appear in the Gaussian theory by insertions of bubbles and vertex Fig. 1(c) insertions from the diagrams contributing to the nonoptimized theory. Bubbles or ''cacti'' diagrams, see Fig. 5 are effectively inserted in Eq. (27) by technique known in field theory,[26]

$$f_{\rm eff}=2\log\frac{\varepsilon_1}{4\pi^2}+2f_{\rm 2D}(x),$$

$$x=\frac{\alpha}{\varepsilon_1^2},\varepsilon_1=\frac{1}{2}(\varepsilon_2+\sqrt{\varepsilon_2^2+16\alpha}). \quad (29)$$

TABLE I. Coefficients c_n and z_n in 2D.

n	c_n	z_{n-1}
1	-2	-4
2	-1	-6
3	$\frac{38}{9}$	$-12.239\,721\,181\,139\,888$
4	$-39-\frac{29}{30}$	$-7.508\,888\,400\,035\,477$
5	471.396 594 516 594 46	$-7.349\,933\,383\,279\,474$
6	$-6471.562\,574\,955\,1446$	$-14.152\,646\,217\,045\,422$
7	101 279.327 845 970 63	$-9.961\,364\,397\,930\,787$
8	$-1\,779\,798.787\,594\,7522$	$-9.174\,960\,576\,928\,443$
9	34 709 019.614 363 678	$-15.232\,548\,389\,083\,844$
10	$-744\,093\,435.668\,222\,31$	$-11.629\,924\,499\,110\,746$
11	17 399 454 123.559 521	$-10.839\,981\,752\,5306$
12	$-440\,863\,989\,257.285\,10$	$-15.936\,692\,766\,1989$
13	12 035 432 945 204.531	$-12.753\,308\,785\,106\,007$

Summing up all the insertions of the mass vertex is achieved by

$$\varepsilon_2=\varepsilon+\alpha a_H. \tag{30}$$

We then expand $f_{\rm eff}$ to order α^{n+1}, and then taking $\alpha=1$, to obtain f_n. Calculating f_n that way, we checked that indeed the first three orders agree with the calculation performed by a direct calculation. Here a few more terms are displayed,

$$\tilde{f}_3=\tilde{f}_2-\frac{8133}{5\varepsilon^8}-\frac{2648a_H}{3\varepsilon^7}-\frac{180a_H^2}{\varepsilon^6}-\frac{16a_H^3}{\varepsilon^5}-\frac{a_H^4}{2\varepsilon^4},$$

$$\tilde{f}_4=\tilde{f}_3+\frac{21\,894.3}{\varepsilon^{10}}+\frac{13\,012.8a_H}{\varepsilon^9}+\frac{3089.33a_H^2}{\varepsilon^8}+\frac{360a_H^3}{\varepsilon^7}+\frac{20a_H^4}{\varepsilon^6}+\frac{0.4a_H^5}{\varepsilon^5}. \tag{31}$$

The nth OPT approximant f_n is obtained by minimization of $\tilde{f}_n(\varepsilon)$ with respect to ε,

$$\left(\frac{\partial}{\partial\varepsilon}-\frac{\partial}{\partial a_H}\right)\tilde{f}_n(\varepsilon,a_H)=0. \tag{32}$$

The above equation is equal to $1/\varepsilon^{2n+3}$ times a polynomial $g_n(z)$ of order n in $z\equiv\varepsilon\cdot a_H$. This was proved using the conformal map (see Sec. IV C below) in Ref. 27 even for more general cases. This property simplifies greatly the task: one has to find roots of polynomials rather than solving transcendental equations. There are n (real or complex) solutions for $g_n(z)=0$. However (as in the case of anharmonic oscillator[19]) the best root is the real root with the smallest absolute value. The roots z_n for $n=0$ to $n=12$ are given in Table. I.

We then obtain $\varepsilon(a_T)=(a_T+\sqrt{a_T^2-4z_n})/2$ solving $z_n=\varepsilon\cdot a_H=\varepsilon a_T-\varepsilon^2$. For $z_0=-4$, we obtain the Gaussian result, dashed line marked "T0" on Fig. 1 of Ref. 20.

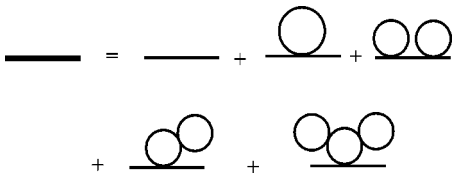

FIG. 5. Summing all bubble diagrams.

B. 3D

In the 3D, the LLL Ginzburg–Landau model, we set

$$K=\frac{1}{4\pi\sqrt{2}}\left(\varepsilon|\psi|^2+\frac{1}{2}|\partial_z\psi|^2\right),$$

$$v=+\frac{\alpha}{4\pi\sqrt{2}}\left[a_H|\psi|^2+\frac{1}{2}|\psi|^4\right], \tag{33}$$

where $a_H=a_T-\varepsilon$ and

$$\psi(x)=\int_{k_3}\int_{\mathbf{k}}\frac{\exp[izk_z]\varphi_{\mathbf{k}}(x)}{(\sqrt{2\pi})^3}\psi(k). \tag{34}$$

The propagator is

$$\langle\psi(k)\psi(l)\rangle=\frac{4\pi\sqrt{2}}{\varepsilon+\frac{k_z^2}{2}}\delta(k+l), \tag{35}$$

or in the coordinate space

$$\langle\psi(x_1,y_1,z_1)\psi(x_2,y_2,z_2)\rangle=\frac{\sqrt{2}}{\pi}\int_{k_z}\frac{\exp[ik_z(z_1-z_2)]}{\varepsilon+\frac{k_z^2}{2}}\exp\left[-\frac{i}{2}(x_1-x_2)(y_1+y_2)\right]\times\exp\left\{-\frac{1}{4}[(x_1-x_2)^2+(y_1-y_2)^2]\right\}. \tag{36}$$

Thus the propagator in the coordinate space factorizes into a function of coordinates (x,y) perpendicular to magnetic field and a function of the coordinate z parallel to it. The mass insertion vertex, Fig. 1(c), now has a value of $(\alpha/4\pi\sqrt{2})a_H$, while the four line vertex is $(\alpha/8\pi\sqrt{2})$. The calculation is basically the same as in 2D, the only difference being extra integrations over k_z. However since the propagator factorizes, these integrations can be reduced to corresponding integrations in quantum mechanics of the anharmonic oscillator.[7]

Again we can take an advantage of existing long series of the nonoptimized Gaussian expansion.[7,24] The results to seventh order are

$$f_{\rm eff}=4\sqrt{\varepsilon}+4\sqrt{\varepsilon}f_{3d}(x),$$

$$f_{\rm 3D}(x)=\sum c_n x^n,\quad x=\frac{1}{2\sqrt{\varepsilon^3}}, \tag{37}$$

TABLE II. Coefficients c_n and z_n in 3D.

n	c_n	z_{n-1}
1	−2	−4
2	−0.5	−5
3	1.583 333 333	−8.803 178 648 215 79
4	−12.667 361 111	−6.187 603 657 880 674
5	125.595 526 19	−5.960 012 621 607 176
6	−1430.592 8959	−9.472 127 468 171 98
7	18 342.765 997	−7.430 474 107 869 646
8	−261 118.677 03	−6.907 260 317 913 621
9	4 084 812.307	−9.819 535 183 5546

where $\sqrt{\varepsilon}$ is given by a solution of the cubic gap equation $(\sqrt{\varepsilon})^3 - a_T\sqrt{\varepsilon} - 4 = 0$,

$$\sqrt{\varepsilon} = a_T(54 + 3\sqrt{324 - 3a_T^3})^{-1/3} + \tfrac{1}{3}(54 + 3\sqrt{324 - 3a_T^3})^{1/3}, \tag{38}$$

and coefficient c_n are listed in Table II. Similarly the OPT formula for the effective energy density can be obtained by using the generational function

$$f_{\text{eff}} = 4\sqrt{\varepsilon_1} + 4\sqrt{\varepsilon_1} f_{3\text{D}}(x), \quad x = \frac{\alpha}{2(\sqrt{\varepsilon_1})^3}, \tag{39}$$

and $\sqrt{\varepsilon_1}$ is given by a solution of equation

$$(\sqrt{\varepsilon_1})^3 - \varepsilon_2\sqrt{\varepsilon_1} - 4\alpha = 0 \tag{40}$$

with $\varepsilon_2 = \varepsilon + \alpha a_H$. The solution of Eq. (40) can be obtained perturbatively in α,

$$\sqrt{\varepsilon_1} = \sqrt{\varepsilon_2} + \frac{2\alpha}{\varepsilon_2} - \frac{6\alpha^2}{\varepsilon_2^{5/2}} + \frac{32\alpha^3}{\varepsilon_2^4} - \frac{210\alpha^4}{\varepsilon_2^{11/2}} + \frac{1536\alpha^5}{\varepsilon_2^7} - \frac{12\,012\alpha^6}{\varepsilon_2^{17/2}} + \frac{98\,304\alpha^7}{\varepsilon_2^{10}} - \frac{831\,402\alpha^8}{\varepsilon_2^{23/2}} + \frac{7\,208\,960\alpha^9}{\varepsilon_2^{13}} + \cdots. \tag{41}$$

Expanding f_{eff} in α to order $n+1$, then one then sets $\alpha = 1$ to obtain $\tilde{f}_n$.

We list here the first few OPT approximants $\tilde{f}_n$,

$$\tilde{f}_0 = 4\sqrt{\varepsilon} + \frac{2a_H}{\sqrt{\varepsilon}} + \frac{4}{\varepsilon},$$

$$\tilde{f}_1 = \tilde{f}_0 - \frac{1}{2\sqrt{\varepsilon^5}}(17 + 8a_H\sqrt{\varepsilon} + a_H^2\varepsilon), \tag{42}$$

$$\tilde{f}_2 = \tilde{f}_1 + \frac{1}{24\varepsilon^4}(907 + 510a_H\sqrt{\varepsilon} + 96a_H^2\varepsilon + 6a_H^3\sqrt{\varepsilon^3}),$$

$$\tilde{f}_3 = \tilde{f}_2 - \frac{228.833\,506\,941\,7501}{\sqrt{\varepsilon^{11}}} - \frac{151.166\,666\,666 a_H}{\varepsilon^5} - \frac{37.1875 a_H^2}{\sqrt{\varepsilon^{11}}} - \frac{4a_H^3}{\varepsilon^4} - \frac{0.156\,25 a_H^4}{\sqrt{\varepsilon^7}}.$$

The OPT nth order result $f_n(a_T)$ is obtained optimizing $\tilde{f}_n$ by varying ε:

$$\left(\frac{\partial}{\partial\varepsilon} - \frac{\partial}{\partial a_H}\right)\tilde{f}_n(\varepsilon, a_H) = 0. \tag{43}$$

Similarly to Eq. (32) in 2D this is equal to $(1/\varepsilon^{(3n/2)+2})g_n(z)$, where now $z \equiv a_H\sqrt{\varepsilon}$ and $g_n(z)$ is a rank n polynomial. Solving $g_n(z)$ and choosing a real root with the smallest absolute value,[19] we obtain z_n listed in Table II up to $n=8$. Then we solve for $\sqrt{\varepsilon}$ the equation $z = a_H\sqrt{\varepsilon} = (a_T - \varepsilon)\sqrt{\varepsilon}$. The solution is

$$\sqrt{\varepsilon} = 2^{1/3}a_T(-27z + \sqrt{-108a_T^3 + 729z^2})^{-1/3} + \frac{1}{32^{1/3}}(-27z + \sqrt{-108a_T^3 + 729z^2})^{1/3}. \tag{44}$$

C. Rate of convergence of OPE

The remarkable convergence of OPE in simple models was investigated in numerous works.[18,27] It was found that at high orders the convergence of partition function of simple integrals (similar to the "zero-dimensional GL" studied in Ref. 9),

$$Z = \int_{-\infty}^{\infty} d\varphi\, e^{-(a\varphi^2 + \varphi^4)}$$

is exponentially fast. The remainder in bound by[18,27]

$$r_N = |Z - Z_N| < c_1 \exp[-c_2 N].$$

For anharmonic oscillator (both positive and negative quadratic term) it is just a bit slower:

$$R_N = |E - E_N| < c_1 \exp[-c_2 N^{1/3}],$$

where E is the ground state energy. We follow here the convergence proof of Ref. 27. The basic idea is to construct a conformal map[28] from the original coupling g to a coupling of bounded range and isolate a nonanalytic prefactor. Suppose we have a perturbative expansion (usually asymptotic, sometimes non-Borel summable)

$$E(g) = \sum_{n=0}^{\infty} c_n g^n.$$

One defines a set of conformal maps dependent on parameter ρ of coupling g onto new coupling β:

$$\overline{g}(\beta, \rho) = \rho\frac{\beta}{(1-\beta)^\kappa}.$$

While range of g is the cut complex plane, the range of β is compact and has an apple like shape (see Fig. 1 of the second paper in Ref. 27). The value of parameter ρ for each approximant will be defined later. Then one defines a scaled energy

$$\Psi(\beta,\rho)=(1-\beta)^{\sigma}E(\bar{g}(\beta,\rho)),$$

where the prefactor $(1-\beta)^{\sigma}$ is determined by strong coupling limit so that $\Psi(\beta,\rho)$ is bounded everywhere. Approximants to Ψ are expansion to Nth order in β,

$$\Psi_N(\beta,\bar{\rho})=\sum_{n=0}^{N}\frac{1}{n!}\frac{\partial^n}{\partial\beta^n}[(1-\beta)^{\alpha}E(\bar{g}(\beta,\bar{\rho}))],$$

with parameter $\bar{\rho}$ substituted by

$$\bar{\rho}=\frac{g}{\beta}(1-\beta)^{\kappa}.$$

The energy approximant becomes

$$E_N(\beta)=\frac{\Psi_N(\beta)}{(1-\beta)^{\sigma}}.$$

Two exponents $\sigma=\frac{1}{2}$ and $\kappa=\frac{3}{2}$, for example, anharmonic oscillator and 3D GL model. OPE is equivalent to choosing β which minimizes $E_N(\beta)$. It can be shown quite generally (see Appendix C of second paper in Ref. 27 and Ref. 19) that the minimization equation is a polynomial one in ρ. This is in line with our observation in previous sections that minimization equations are polynomial in z with ρ identified as $-1/z$.

The remainder $R_N=|E-E_N|$ using dispersion relation is bounded by

$$R_N<c_1 g^{\sigma/\kappa}(\bar{\rho}N^b)^N+c_2\exp\left[-N\left(\frac{\bar{\rho}}{g}\right)^{1/\kappa}\right],$$

where exponent b is determined by discontinuity of $E(g)$ at small negative g,

$$\mathrm{Disc}\,E(g)\sim\exp\left[-\frac{\mathrm{const}}{(-g)^{1/b}}\right],$$

where $b=1$ for anharmonic oscillator and $b=3/4$ for 3D GL model.[7] For 3D GL model, we found that $R_N<c_1\times\exp[-c_2N^{1/3}]$ as in the anharmonic oscillator.

V. RESULTS AND COMPARISON WITH OTHER THEORIES AND EXPERIMENTS

A. Energy, precision of OPT

In Fig. 1 of Ref. 20 we present OPT for orders $n=0$ (Gaussian), 1,3,4,5,6,8,9,12 together with several orders ($T0,\ldots,T12$) of the nonoptimized high temperature expansion in 2D. The values of free energy of 2D and 3D models for several a_T are tabulated in Table III and Table IV, respectively. One clearly observes that in 2D the OPT series converge above $a_T=-2.5$ and diverge below $a_T=-3.5$. On the other hand, the nonoptimized series never converge despite the fact that above $a_T=2$ first few approximants provide a quite precise estimate consistent with OPT. Above $a_T=4$ the liquid becomes essentially a normal metal and fluctuations effects are negligible (see Fig. 2 of Ref. 20 and Fig. 7) and are hard to measure. Therefore the information the OPT provides is essential to compare with experiments on magnetization and specific heat.

TABLE III. Free energy f_n at different orders (a constant $-2\log 4\pi^2$ was subtracted).

a_T	-2	-1.5	-1	-0.5
f_0	$-2.194\,16$	$-1.429\,41$	$-0.749\,027$	$-0.146\,255$
f_1	$-2.775\,16$	$-1.805\,56$	$-0.988\,706$	$-0.297\,222$
f_3	$-2.538\,54$	$-1.682\,94$	$-0.925\,643$	$-0.264\,857$
f_4	$-2.558\,89$	$-1.691\,43$	$-0.929\,12$	$-0.266\,258$
f_6	$-2.700\,76$	$-1.740\,15$	$-0.945\,544$	$-0.271\,734$
f_7	$-2.624\,47$	$-1.718\,22$	$-0.939\,384$	$-0.270\,031$
f_9	$-2.515\,33$	$-1.692\,3$	$-0.933\,365$	$-0.268\,653$
f_{10}	$-2.599\,43$	$-1.709\,44$	$-0.936\,772$	$-0.269\,318$
f_{12}	$-2.726\,13$	$-1.731\,13$	$-0.940\,395$	$-0.269\,915$

If precision is defined as $(f_{12}-f_{10})/f_{10}$, we obtain 4.87%,1.27%,0.387%,0.222%,0.032% at $a_T=-2,-1.5,-1,-0.5,0$, respectively. We choose approximants $n=0,1,3,4,6,7,9,10,12$ because they are "the best roots" in a sense defined in Ref. 19, Chapt. 5. For comparison with other theories and experiments on Fig. 2 of Ref. 20 and Fig. 7 we use the 10th approximant.

In 3D the picture is much the same, see Fig. 6. The series converge above $a_T=-4.5$ and diverge below $a_T=-5.5$. The nonoptimized series are useful only above $a_T=-1$.

We define the precision as $(f_7-f_4)/f_7$. f_4 and f_7 are the best roots among the sequences. Then we obtain 6.55%,2.94%,0.0247%,0.007 792 22%, at $a_T=-5,-3,-1.5,-1$, respectively.

B. Other theories

We compare with other theoretical treatments of the same model. A direct method is the Monte Carlo simulation of the same model. The 2D model was simulated by Moore, Kato, and Nagaosa, and Hu MacDonald. The circles on Fig. 7 for specific heat are the results of the Monte Carlo simulation of

TABLE IV. Free energy f_n at different orders for 3D.

a_T	-5	-3	-1.5	-1
f_0	$-4.733\,13$	0	2.657 63	3.411 12
f_1	-6.493	$-0.375\,697$	2.539 01	3.328 29
f_2	$-6.925\,85$	$-0.427\,383$	2.5287	3.3222
f_3	$-5.275\,95$	$-0.280\,923$	2.555 51	3.338
f_4	$-5.680\,59$	$-0.292\,936$	2.554 55	3.337 57
f_5	$-4.680\,76$	$-0.265\,834$	2.556 47	3.338 39
f_6	$-7.326\,54$	$-0.313\,048$	2.553 64	3.337 22
f_7	$-5.331\,49$	$-0.301\,797$	2.553 92	3.337 31
f_8	$-8.019\,07$	$-0.316\,175$	2.553 59	3.3372

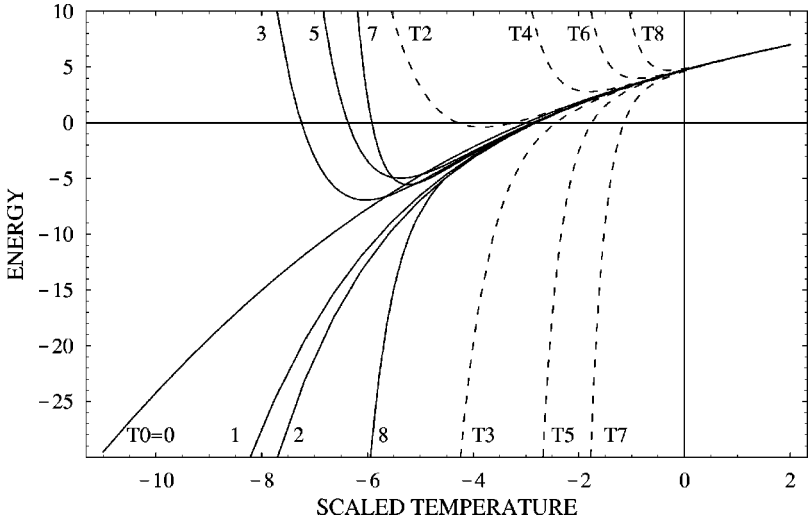

FIG. 6. The 3D OPT energy and nonoptimized energy at different orders (denoted by numbers and "*T*" plus numbers, respectively). One can see clearly OPT series are convergent, for example, at $a_T=-5$.

the LLL system by Kato and Nagaosa in Ref. 15 performed with 256 vortices. In 3D the model was simulated with 100 vortices by Sasik and Stroud,[16] magnetization data are compared with our results on Fig. 8.

An analytic theory used successfully to fit the magnetization and the specific heat data[29] was developed in Ref. 13. Their free energy density is

$$f_{\rm eff}=-\frac{a_T^2U^2}{4}+\frac{a_TU}{2}\sqrt{\frac{U^2a_T^2}{4}+2}+2\,\mathrm{arcsinh}\left[\frac{a_TU}{2\sqrt{2}}\right],$$

$$U=\frac{1}{2}\left[\frac{1}{\sqrt{2}}+\frac{1}{\sqrt{\beta_A}}+\tanh\left[\frac{a_T}{4\sqrt{2}}+\frac{1}{2}\right]\left(\frac{1}{\sqrt{2}}-\frac{1}{\sqrt{\beta_A}}\right)\right]. \quad (45)$$

The corresponding magnetization and specific heat are shown as dashed lines in Fig. 2 of Ref. 20 and Fig. 7, respectively. The theory applies not only to the liquid phase, but also to the solid although the transition is not seen (should be considered as a 2% effect not determined by the theory). At large positive a_T neglecting the exponentially small contributions to U, one obtains

$$f_{\rm eff}=-\frac{a_T^2}{8}+\frac{a_T}{2\sqrt{2}}\sqrt{\frac{a_T^2}{8}+2}+2\,\mathrm{arcsinh}\left[\frac{a_T}{4}\right]$$

$$=1-2\log 2+2\log a_T+\frac{4}{a_T^2}-\frac{16}{a_T^4}+\frac{320}{3a_T^6}. \quad (46)$$

On the other hand, the high temperature expansion of the optimized Gaussian is

$$-2\log 4\pi^2+2\log a_T+\frac{4}{a_T^2}-\frac{18}{a_T^4}+\frac{1324}{9a_T^6}. \quad (47)$$

One observes that the high temperature expansion of two theories are in remarkable agreement up to the order $1/a_T^4$.

C. Magnetization, 2D

Experiments on great variety of layered high Tc cuprates (Bi or Tl[5] based) show that in 2D, magnetization curves for different applied field intersect at a single point (M^*,T^*). The range of magnetic fields is surprisingly large (from sev-

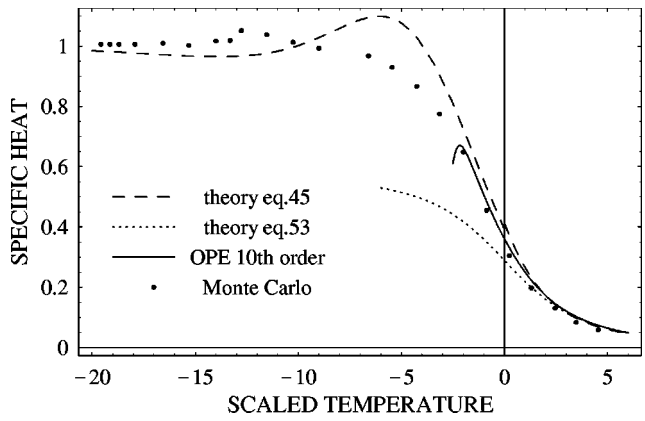

FIG. 7. The 2D specific heat. The Monte Carlo data by Kato and Nagaosa in Ref. 15 (points), specific heat from OPT for $n=10$ (the solid line), from phenomenological formula (the dotted line), and Tesanovic *et al* (Ref. 13) theory (the dashed line).

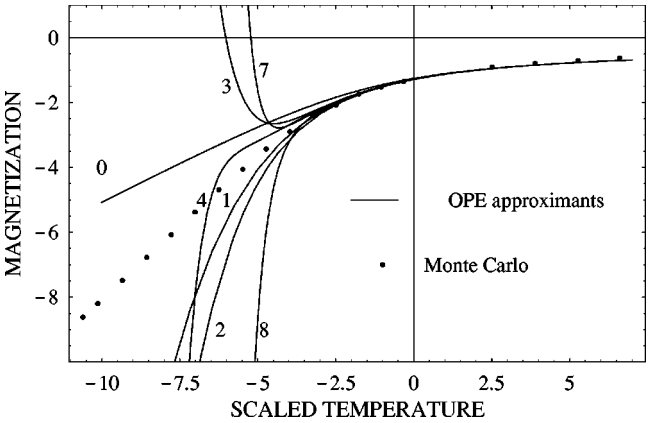

FIG. 8. The 3D magnetization plot. The Monte Carlo data by Sasik and Stroud in Ref. 15 (points), specific heat from OPT of different OPE approximants are denoted by numbers. The best approximants are $n=4,7$ (solid line).

eral hundred Oe to several Tesla). Assuming this it is easy to derive the scaled LLL magnetization just from the existence of the point. The dimensionless LLL magnetization is defined as[30]

$$m(a_T) = -\frac{df_{\rm eff}(a_T)}{da_T} \tag{48}$$

and the measure magnetization is

$$4\pi M = -\frac{e^* h}{c m_{ab}} \langle |\psi|^2 \rangle = -\frac{e^* h}{c m_{ab}} |\psi_r|^2 \left(\frac{2\alpha T_c}{b'} \right) \sqrt{\frac{b\omega}{4\pi}}, \tag{49}$$

where ψ is the order parameter of the original model, and ψ_r is the rescaled one, which is equal to $[df_{\rm eff}(a_T)]/da_T$. Thus

$$4\pi M = \frac{e^* h}{c m_{ab}} \left(\frac{2\alpha T_c}{b'} \right) \sqrt{\frac{b\omega}{4\pi}} m(a_T). \tag{50}$$

Using the definition of $a_T = -\eta[(1-t-b)/\sqrt{bt}]$, $\eta = (2\pi^2 Gi)^{-1/4}$, b can be written as

$$b = t\left(\frac{a_T}{2\eta} \pm \sqrt{\frac{1-t}{t} + \frac{a_T^2}{4\eta^2}} \right)^2. \tag{51}$$

Thus Eq. (50) implies that

$$\begin{aligned} m(a_T) &= \frac{4\pi c m_{ab} M}{e^* h} \frac{b'}{2\alpha T_c} \frac{\eta}{\sqrt{bt}} \\ &= \frac{4\pi c \eta m_{ab} M}{e^* h t} \frac{b'}{2\alpha T_c} \frac{1}{\left| \sqrt{\frac{1-t}{t} + \frac{a_T^2}{4\eta^2}} \pm \frac{a_T}{2\eta} \right|} \\ &= \frac{4\pi c m_{ab} M \eta}{e^* h |1-t|} \frac{b'}{2\alpha T_c} \left| \sqrt{\frac{1-t}{t} + \frac{a_T^2}{4\eta^2}} \pm \frac{a_T}{2\eta} \right|. \end{aligned} \tag{52}$$

If we assume that the experimental observation that all the magnetization curves intersect at some point (T^*, M^*), $m(a_T)$ is

$$m(a_T) = C_1(a_T \pm \sqrt{C_2 + a_T^2}), \tag{53}$$

$$C_1 = \frac{2\pi c m_{ab} M^*}{e^* h |1-t^*|} \frac{b'}{2\alpha T_c}, \quad C_2 = 4\eta^2 \frac{1-t^*}{t^*}.$$

On the other hand, if we require that the first two terms of the high temperature expansion of Eq. (53) and the high temperature expansion of the magnetization are equal, one finds that

$$C_1 = \tfrac{1}{4}, \quad C_2 = 16.$$

When we plot this line on Fig. 2 of Ref. 20 (the dotted line) we find that at lower temperatures the magnetization is overestimated. On the other hand, magnetization of the theory of Tesanovic *et al.* (the dashed line on Fig. 2 of Ref. 20) underestimate the magnetization. The OPE results are consistent with the data within the precision range until the radius of convergence $a_T = -3$. It is important to note that deviations of both the phenomenological formula Eq. (53) and the Tesanovic's are clearly beyond our precision range.

We conclude therefore that although the theory of Tesanovic *et al.* is very good at high temperatures (deviations only at the order $1/a_T^4$) they become of the order 5–10% at $a_T = -3$. The advantage of this theory is however that it interpolated smoothly to the solid and never deviates more than 10%. The coincidence of the intersection of all the lines at the same point (T^*, M^*) cannot be exact. Like in 3D it is just approximate, although the approximation is quite good especially at high magnetic fields.

D. Specific heat, 2D

The specific heat OPE result is compared in Fig. 7 with Monte Carlo simulation of the same model by Kato and Nagaosa[15] (black circles), the phenomenological formula following from Eq. (53) (dotted line), and the theory of Tesanovic *et al.*[13] (dashed line). The agreement with the direct MC simulation is very good.

E. Magnetization in 3D

We compare here our results on the LLL scaled magnetization with the Monte Carlo simulation of the LLL system by Sasik and Stroud.[16] They are actually more precise in 3D. Figure 8 contains several OPE approximants ($n = 0,1,2,3,4,7,8$) and their data on all three magnetic fields (representing $2T, 3T$, and $5T$ in model YBCO). According to the criterion of the ''best root'' the best approximant should be $n = 7$. Clearly up to the radius of convergence the agreement is within the expected precision.

VI. CONCLUSION

In this paper we obtained the optimized perturbation theory results for both the 2D and the 3D LLL model. It allows to obtain a convergent series (rather than asymptotic). The magnetization and specific heat of vortex liquids with definite precision are calculated. On the basis of this one can make several definitive qualitative conclusions. The intersection of the magnetization lines is only approximate not only in 3D (the result already observed in Monte Carlo simulation[16]), but also in 2D. The theory by Tesanovic,[13] which uses completely different ideas, describes the physics remarkably well in high temperatures and deviates on the 5–10% precision level at $a_T = -2$ in 2D.

ACKNOWLEDGMENTS

We are grateful to our colleagues A. Knigavko and T. K. Lee for numerous discussions and encouragement and Z. Tesanovic for explaining his work to one of us and sharing his insight. One of us is grateful to Professor B. Ya. Shapiro and Y. Yeshurun for hospitality at Bar Ilan. The work was supported by NSC of Taiwan grant NSC#89-2112-M-009-039.

*Electronic mail: lidp@mono1.math.nctu.edu.tw
†Electronic mail: baruch@vortex1.ep.nctu.edu.tw

[1] G. Blatter, M.V. Feigel'man, V.B. Geshkenbein, A.I. Larkin, and V.M. Vinokur, Rev. Mod. Phys. **66**, 1125 (1994).
[2] D.R. Nelson, Phys. Rev. Lett. **60**, 1973 (1988); E. Brezin, D.R. Nelson and A. Thiaville, Phys. Rev. B **31**, 7124 (1985).
[3] E. Zeldov, D. Majer, M. Konczykowski, V.B. Geshkenbein, V.M. Vinokur and H. Shtrikman, Nature (London) **375**, 373 (1995).
[4] M. Roulin, A. Junod, A. Erb, and E. Walker, J. Low Temp. Phys. **105**, 1099 (1996); A. Schilling *et al.*, Phys. Rev. Lett. **78**, 4833 (1997).
[5] R. Jin, A. Schilling, and H.R. Ott, Phys. Rev. B **49**, 9218 (1994); P.H. Kes *et al.*, Phys. Rev. Lett. **67**, 2383 (1991); A. Wahl *et al.*, Phys. Rev. B **51**, 9123 (1995).
[6] U. Welp *et al.*, Phys. Rev. Lett. **67**, 3563 (1991).
[7] D.J. Thouless, Phys. Rev. Lett. **34**, 946 (1975); G.J. Ruggeri and D.J. Thouless, J. Phys. F: Met. Phys. **6**, 2063 (1976).
[8] G.J. Ruggeri, Phys. Rev. B **20**, 3626 (1979).
[9] N.K. Wilkin and M.A. Moore, Phys. Rev. B **47**, 957 (1993).
[10] T.J. Newman and M.A. Moore, Phys. Rev. B **54**, 6661 (1996).
[11] J. Yeo and M.A. Moore, Phys. Rev. Lett. **76**, 1142 (1996); Phys. Rev. B **54**, 4218 (1996).
[12] I. Affleck and E. Brezin, Nucl. Phys. B **257**, 451 (1985); L. Radzihovsky, Phys. Rev. Lett. **74**, 4722 (1995).
[13] Z. Tesanovic, L. Xing, L. Bulaevskii, Q. Li, and M. Suenaga, Phys. Rev. Lett. **69**, 3563 (1992); Z. Tesanovic and A.V. Andreev, Phys. Rev. B **49**, 4064 (1994).
[14] L. Bulaevskii, M. Ledvij, and V.G. Kogan, Phys. Rev. Lett. **68**, 3773 (1992).
[15] Y. Kato and N. Nagaosa, Phys. Rev. B **48**, 7383 (1993); J. Hu and A.H. MacDonald, Phys. Rev. Lett. **71**, 432 (1993); J.A. ONeill and M.A. Moore, Phys. Rev. B **48**, 374 (1993).
[16] R. Sasik and D. Stroud, Phys. Rev. Lett. **75**, 2582 (1975).
[17] P.W. Stevenson, Phys. Rev. D **23**, 2916 (1981); A. Okopinska, *ibid.* **35**, 1835 (1987).
[18] A. Duncan and H.F. Jones, Phys. Rev. D **47**, 2560 (1993); C.M. Bender, A. Duncan, and H.F. Jones, *ibid.* **49**, 4219 (1994); B. Bellet, P. Garcia, and A. Neveu, Int. J. Mod. Phys. A **11**, 5587 (1996); **11**, 5607 (1996).
[19] H. Kleinert, *Path Integrals in Quantum Mechanics, Statistics, and Polymer Physics*, (World Scientific, Singapore, 1995).
[20] D. Li and B. Rosenstein, Phys. Rev. Lett. **86**, 3618 (2001).
[21] D. Li and B. Rosenstein, Phys. Rev. B **60**, 9704 (1999).
[22] D.J. Thouless, Phys. Rev. Lett. **34**, 946 (1975); A.J. Bray, Phys. Rev. B **9**, 4752 (1974).
[23] R.P. Feynman, *Statistical Mechanics* (Benjamin, Reading, MA, 1972).
[24] S. Hikami, A. Fujita, and A.I. Larkin, Phys. Rev. B **44**, R10400 (1991); E. Brezin, A. Fujita, and S. Hikami, Phys. Rev. Lett. **65**, 1949 (1990); **65**, 2921(E) (1990).
[25] J. Hu, A.H. MacDonald, and B.D. Mckay, Phys. Rev. B **49**, 15263 (1994).
[26] T. Barnes and G.I. Ghandour, Phys. Rev. D **22**, 924 (1980); A. Kovner and B. Rosenstein, *ibid.* **39**, 2332 (1989); **40**, 504 (1989).
[27] R. Guida, K. Konishi, and H. Suzuki, Ann. Phys. (N.Y.) **241**, 152 (1995); **249**, 109 (1996).
[28] R. Seznec, and J. Zinn-Justin, J. Math. Phys. **20**, 1398 (1979).
[29] S.W. Pierson, O.T. Valls, Z. Tesanovic, and M.A. Lindermann, Phys. Rev. B **57**, 8622 (1998); S.W. Pierson and O.T. Valls, *ibid.* **57**, 8143 (1998); A. Carrington, A.P. Mackenzie, and A. Tyler, *ibid.* **54**, 3788 (1996).
[30] Dingping Li and B. Rosenstein, following paper, Phys. Rev. B **65**, 024514 (2001).